IEEE Access
Multidisciplinary | Rapid Review | Open Access Journal

Received February 21, 2020, accepted March 12, 2020, date of publication March 16, 2020, date of current version March 30, 2020.

Digital Object Identifier 10.1109/ACCESS.2020.2981300

Chest Wearable Apparatus for Cuffless Continuous Blood Pressure Measurements Based on PPG and PCG Signals

DAVIDE MARZORATI[1], DARIO BOVIO[2], CATERINA SALITO[1,2], LUCA MAINARDI[1], AND PIETRO CERVERI[1]

[1]Department of Electronics, Information and Bioengineering, Politecnico di Milano, 20133 Milan, Italy
[2]Biocubica SRL, 20154 Milan, Italy

Corresponding author: Pietro Cerveri (pietro.cerveri@polimi.it)

ABSTRACT This paper describes an integrated chest wearable apparatus for continuous blood pressure (BP) measurements exploiting the heart-rate (HR) and the pulse arrival time (PAT) in a modified Moens-Korteweg model. The device embeds a miniaturized gas pressure sensor to record the phonocardiogram (PCG) of the heart sounds, a LED-photodiode pair to detect the photoplethysmogram (PPG) of the blood flow wave, a μ-controller, a wireless communication module and the power supply. With the proposed device no active participation would be required from human subjects for BP measurements, since the HR and the PAT are continuously extracted from the PCG and PPG signals. Dedicated signal processing algorithms were developed and implemented off-line to extract both HR and PAT. A subject-specific calibration protocol of the BP model was designed and implemented. The calibration and validation of the apparatus were performed on a cohort of 20 healthy subjects. A GIMA ABPM pressure Holter was chosen as reference device, and 8 measurements points, evenly distributed over a 10-minute interval, were used for model calibration for each subject. The range of DBP and SBP measurements were 52-85 mmHg and 90-141 mmHg, respectively. The results from Bland-Altman analysis showed that the mean$\pm$1.96SD for the estimated diastolic, systolic, and mean BP with the proposed method against reference were 0.01$\pm$7.55, 1.47$\pm$3.76, 0.74$\pm$4.38 mmHg, respectively. The corresponding mean absolute differences (MAD) were 3.06, 1.83, and 1.80 mmHg. These results demonstrates that the acquisition apparatus is able to continuously estimate the BP with an accuracy comparable to traditional cuff-based devices.

INDEX TERMS Wearable device, blood pressure measurement, pulse transit time (PTT), pulse arrival time (PAT), integrated system.

I. INTRODUCTION

Wearable devices for cuff-less blood pressure estimation (BP), as in ambulatory blood pressure measurement (ABPM), have been the subject of intensive investigations due to their potential ability to provide continuous measurements over a long time period (24-48 hours), in different postures or even during different physical activities [1]–[8]. The operating principle of the majority of such devices is based on the non-invasive measurement of intermediate physiological quantities, such as the R-wave peak extracted from the electrocardiogram (ECG) and arrival time of the blood pulse (PAT) at a peripheral site, measured by the photoplethysmogram (PPG), and on mathematical models that bind together such quantities to the BP [9]–[13]. Traditionally, the PAT has been considered an adequate surrogate of the pulse transit time (PTT), defined as the time taken by the blood pulse that spreads from a proximal to a peripheral site, which has been shown to correlate well with changes in BP over a wide physiological BP range [14]–[16]. In this paradigm, the Moens-Korteweg (M-K) model [17], [18] links the velocity of the blood pulse (PWV) propagating through an arterial tract of length L to its geometric and mechanical parameters as:

$$PWV = \frac{L}{PTT} = \sqrt{\frac{Eh}{2r\rho}} \tag{1}$$

The associate editor coordinating the review of this manuscript and approving it for publication was Mohsin Jamil.

where E, h, r and ρ are the elasticity (Young modulus), the thickness, the inner radius and the density of the vessel, respectively. Being the elasticity strictly correlated to the blood pressure by means of a scalar factor a as the following heuristic equation suggests [19]:

$$E = E_0 e^{aBP} \tag{2}$$

then BP can be resolved in:

$$BP = -\frac{2}{a} \ln PAT + \frac{\ln \frac{2r\rho L^2}{hE_0}}{a} \tag{3}$$

where the PTT has been substituted by the PAT. Technically, the arrival time at a peripheral site can be computed from a characteristic point of the PPG, namely the signal foot [11]. PPG signal is acquired using a LED coupled to a photodiode, which are placed on a superficial skin site like the fingertip, exploiting transmissive PPG, or on the wrist or sternum, exploiting, instead, reflective PPG. In particular, the reliability of the reading at the capillary arteries of the sternum surface was supported by the fact that the blood pulse speed is mainly related to the propagation characteristics of the elastic central arteries (aorta and carotid) [20]–[22]. This makes the PAT measured at the sternum consistent with the mathematical model in (3) that holds mainly for central arteries. In order to avoid the use of the ECG signal, the detection of the first heart sound (*S1*) in the phonocardiogram (PCG) was proposed in substitution of the R-wave peak, thus avoiding the explicit measure of ECG that, even for a single derivation, requires a differential acquisition and an active participation of the subject, thus preventing a continuous BP measurement [23], [24]. In such a case, the PAT is the time delay between the beginning of the systole, marked by the mitral valve closure sound, and the arrival of a pulse detected on the PPG (Fig. 1), identified again by the PPG foot [11], [24]–[26]. Acoustic sensors located on the chest, in the proximity of the heart, were proposed to detect the PCG [19], [24]. Considering an explicit effect of the heart rate on the BP [27]–[30], (3) can be rewritten as:

$$BP = \alpha \ln PAT + \beta f(HR) + \gamma \tag{4}$$

where f is a function to be set and the three scalar parameters α, β and γ are to be estimated on an individual basis by means of a minimum amount of known BP values read concurrently with the PAT. In principle, such a model holds for both systolic (SBP) and diastolic (DBP) pressures. Commercial smartwatches, as the Heartisans (Heartisans, Hong Kong) and CareUp (Farasha Labs, Paris, France) have been recently proposed on the market exploiting PPG and ECG, along with models based on (4), to provide BP values on demand. However, they are not able to address continuous long-term measurements, which are fundamental for diagnostic monitoring [4], [14]. This issue was addressed originally by a chest sensor as a proof-of-concept [21] and only recently feasibility studies have been proposed [22], [31]. Some technical (e.g. sensor reliability and robust measurements for long-term monitoring) and ergonomic (e.g. device shape and positioning on the thorax) challenges still prevent the development of such chest-based devices ready for pre-clinical validation.

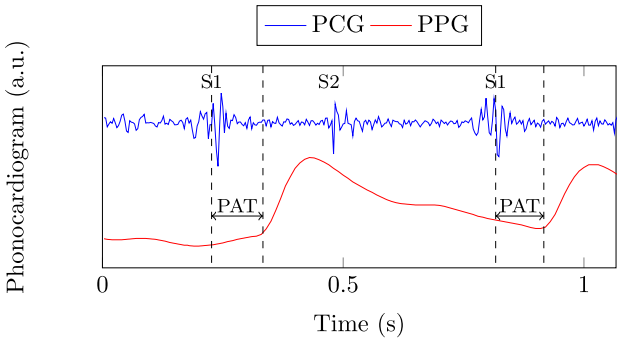

FIGURE 1. PAT calculation starting from phonocardiographic (PCG) and photoplethysmographic (PPG) signals. By identifying the closing of the atrioventricular valves (heart sound *S1*) and the foot value of the PPG signal, it is possible to estimate the value of pulse arrival time (PAT). Heart sound *S2*, representing the closing of the semilunar valves, is also reported in the figure.

To bridge this gap, in this paper we present an innovative device to be located at the subject chest able to record the PPG and the PCG signals, detect the heart sound *S1*, calculate the beat-by-beat PAT, and finally compute the BP. The proposed apparatus incorporated a miniaturized pressure sensor to acquire the PCG and reduce effects of environmental sound noise, an optical system to acquire the PPG, one μ-controller, one wireless communication module, an internal memory for data storage and the power supply. Three main technical innovations, subject of a patent pending at European scale (Patent No. EP3248541A1) by our group, are here presented: a) the design of a custom system to detect heart sounds by acquiring air pressure signals at the chest interface; b) the on-chip development of the required analog front-end components by leveraging on the FPGA-based μ-controller architecture; c) the optimized hardware implementation featuring low power consumption that allowed continuous signal recording up to 10 hours. Preliminary tests about the quality of the BP measure harnessing the model described in (4) were carried out on healthy and normotensive subjects according to a predefined acquisition protocol.

II. MATERIALS AND METHODS

A. DEVICE REQUIREMENTS AND COMPONENT SETUP

Specific technical requirements, summarized in Table 1, guided the design and the development of the integrated device. First, the demand of long time data recording (up to 12 consecutive hours) posed constraints on the power consumption. Second, the potential great amount of recorded data required an on-board memory. Assuming to store 1K samples per second for both PCG and PPG signals, a shared sampling of 1KHz and a storage capacity on board of at least 400MB were required. Third, in order to be worn during night and day, in different activity conditions, specific wearability and ergonomic criteria were taken into account. Moreover, the concurrent detection of PPG and PCG, with

TABLE 1. Device technical requirements.

Requirement	Proposed Solution
24-Hour data storage	On-Board SD Card
Communication with host	Bluetooth communication
Long battery duration	Low power μ-controller, minimal analog front end, and Bluetooth Low Energy protocol
Minimal human intervention	Pressure sensor for heart sound recordings (no ECG required)
Ergonomics	Lightweight and wearable

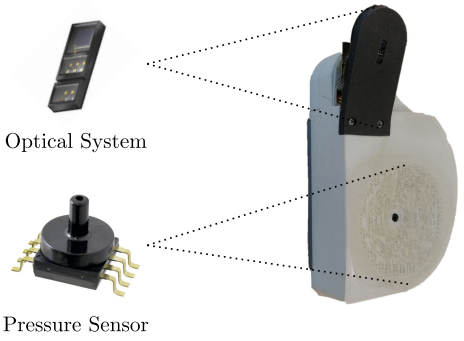

FIGURE 2. Top left: SFH 7060 optical system by BioMon Sensor devoted to PPG detection. Bottom left: MPXV7002 integrated silicon pressure sensor from NXP® Semiconductors devoted to PCG detection. Right: front view of the developed device showing the optical sensing area (black) and the pressure sensing area (bell shape). Overall, the device features a height of about 6cm, a width at the base of 4.5cm, a thickness of 1.5cm, and a weight of approximately 100 gr.

particular focus on the first heart sound $S1$, required to locate the device in contact with the chest surface. As a consequence, the device was designed to encapsulate one optical and one acoustic sensor devoted to the acquisition of the two signals (Fig. 2). The chosen SFH 7060 system (BioMon Sensor - Osram) is an analog multi-chip optical sensor embedding a wide-range photodiode (400-1100nm), with good spectral sensitivity (0.5A/W), and three green LED emitters (λ_{PEAK} = 530nm), along with one red (λ_{PEAK} = 660nm) and one infrared (λ_{PEAK} = 950nm) emitters. In accordance with recent literature findings, only green light was used [32]–[34]. In order to detect heart sounds, atmospheric pressure measurements were considered instead of traditional acoustic sensing, which have been shown to be very prone to the environmental noise. The underlying idea was to detect the air pressure variation at the skin interface transmitted by the inner sound propagation. The technical solution consisted in coupling together the MPXV7002 analog pressure sensor (NXP Semiconductor) and a custom-designed amplification chamber (resembling a bell-shaped stethoscope) into a differential pressure setup, that is the pressure measured by the sensor into the bell was referenced to the local atmospheric pressure (Table 2). The shape of the device, conceived to ensure ergonomic contact with the skin, featured a circular base for the stethoscope chamber in the bottom part and a superior narrow part holding the optical sensor (Fig. 2). Operationally, the stethoscope part was placed close to the left side of the chest while the optical part close to the sternum region, at a distance of about 50mm in between by design. While the stethoscope part, as well as the case for the electronics and the battery, had to be rigid for the sound transmission requirement, the material for the PPG sensor holder was made of soft silicon rubber equipped with an elastic metallic coil. This way, the flexibility of the optical chassis, joined to force exerted by the coil, allowed for a better coupling of the optical sensor to the chest conformation. In order to avoid the real-time transmission of the acquired signals, a 8GB microSD card was used. The device embedded a wireless communication module implementing a Bluetooth Low Energy (BLE) protocol by means of the CYBLE-222014 module (Cypress, USA). At this preliminary stage of development, the BLE module was used to check the quality of the sampled PPG and PCG signals through a custom software running on an host machine, and for sending/receiving commands from the operator using the device. The power supply was ensured by a single 1.5V AA Litium battery, along with one analog and one digital voltage regulation circuitry (Fig. 3). In order to supply both digital (3V) and analog (5V) components, using the 1.5V battery, two boost converters from Texas Instruments were used. In particular, TPS61021A for the digital part (efficiency of 0.9 at 1.2V) and TPS61072 for the analog one (efficiency of 0.83 at 1.2V).

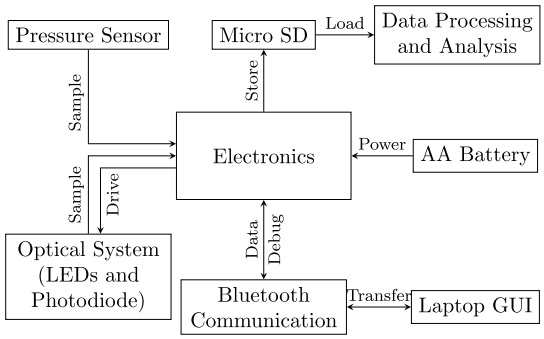

FIGURE 3. Block diagram of the components involved in the device. The main electronic core, powered by a single 1.5V battery, handles the analog reading of the pressure sensor and of the photodiode, storing the sampled data on a μSD card. Furthermore, the micro-controller drives the LEDs of the optical system, and allows a communication, via Bluetooth Low Energy, with a host device. At the time of writing, data processing and analysis is performed offline.

B. CIRCUITRY

The electronic components of the device were embedded in two different printed circuit boards (PCB): the main acquisition and processing (AP) board (Fig. 4a and 4b) and the optical system (OS) board (Fig. 4c), whose shapes were designed to feature the custom footprint of the geometric shape of the device. The OS board enclosed the optical sensor and the driving components, while the AP board featured the micro-controller, the communication module, the SD

TABLE 2. Technical details of the hardware components.

PRESSURE SENSOR (M1XV-7002 NXP Semiconductors, The Netherlands)			
Range: ±2kPa	*Voltage Supply*: 5V	*Sensitivity:* 1V/1kPa	*Size:* 11.3×18.2×12.9mm
OPTICAL SENSOR (SFH 7060 BioMon Sensor - Osram, DE)			
Max Sensitivity: $\lambda = 900$nm	*Light*: 3 LEDs (λ=530nm)	*Forward current:* 15mA	*Size:* 7.2×2.5×0.9mm
BOOST CONVERTER (TPS61021A/TPS6102072, Texas Instruments, USA)			
Analog: TPS6102072	*Efficiency*: 0.83 at 1.2 V	*Digital:* TPS61021A	*Efficiency:* 0.9 at 1.2V
COMMUNICATION (CYBLE-222014, Cypress, USA)		**ON-BOARD MEMORY (μSD, 3M, USA)**	
Format: BLE 4.2	*Interface:* SPI	*Space:* 8GB	*Interface:* SPI
μC (CY8C5888LTI-LP097, Cypress, USA)		**PRINTED CIRCUIT BOARD**	
Architecture: Cortex M3	*Package:* QFN-68	*Main board:* 4 layers	*Optical board:* 4 layers

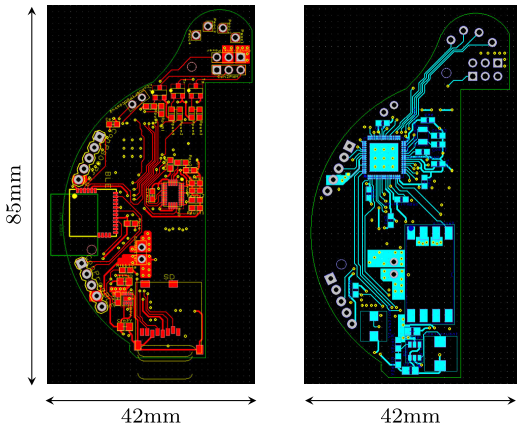

(a) AP board top layer. (b) AP board bottom layer.

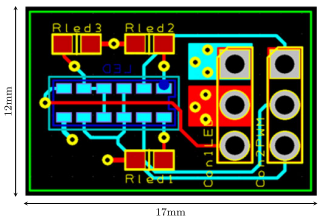

(c) Optical board top and bottom layers.

FIGURE 4. PCB design of the acquisition and processing board and the optical board. Without lack of generality, ground and power supply layers were not depicted in figure.

card, the voltage conditioning circuit, the pressure sensor and the corresponding front-end. The programmable system on chip (PSoC) CY8C5888LTI-LP097 (Cypress, USA) is a micro-controller that we adopted as main core of the device. The PSoC is based on a 32-bit ARM Cortex-M3 processor and features a programmable FPGA-based system-on-chip with configurable analog and digital blocks. Using a PSoC μ-controller, all the analog components required for the front-end of analog signals were moved directly on the FPGA chip, thus reducing the size and the cost of the printed circuit boards. Even if this micro-controller is slightly more expensive than traditional micro-controllers, its flexible architecture allowed us to achieve a fast development of the described prototype, since the majority of the analog components were integrated directly on chip. For the analog section, the current needs were mainly estimated in 20 mA for the green LEDs, 10mA for the pressure sensor, about 6mA for the analog supply of the μ-controller, with a total amount of about 36mA. For the digital part, the main needs were 20mA for the digital supply of the μ-controller, an average amount of 10mA for the SD card writing operations, 6mA on average for transmitting and receiving operations of the BLE module. In total, a required maximum average current for the digital subsystem was estimated in 36mA. Considering the capacity of the AA battery (about 2500mAh) and the efficiency of the voltage regulators, the overall requirement of a maximum average current of 250mA allowed in principle ∼10 hours of continuous registration. The PSoC μ-controller, the pressure sensor and the analog boost converters were placed on the bottom layer of the main AP board. The SD card, the digital boost converter, the BLE module and the driving circuit of the optical system were placed on the top layer. Ground and power layers were placed in between the top and bottom layers.

C. PSOC μ-CONTROLLER SETUP

The configuration and programming of the PSoC were performed using PSOC Creator 4.2 IDE (Cypress, USA). The configurable FPGA-based system-on-chip of the PSOC allowed us to implement entirely on-board the analog front-end required for both the pressure sensor and the photodiode and the pulse-width-modulation (PWM) circuit necessary to drive the the green LEDs (Fig. 5). A PWM block was implemented on chip setting a period of 2μs with a 50% duty cycle. The PCG signal was connected to the positive input of a programmable gain amplifier (PGA), configured in low power mode, with an initial gain equal to 0 dB. A digital-to-analog converter ($VDAC_2$ in Fig. 5) was used to drive the negative input of the PGA, as an external voltage reference, in order to remove the sensor offset. Concurrently, the DAC signal drove the negative input of a $\Delta\Sigma$ analog to digital converter (ADC) through a voltage follower to match impedance. The ADC was configured to capture data at sampling

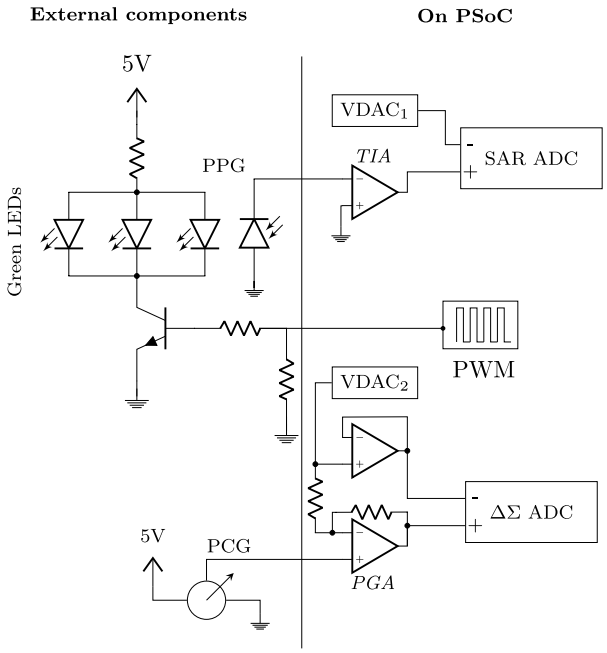

FIGURE 5. Analog front-end of the PCG and PPG signals implemented on the PSoC 5Lp μ-controller and circuit for the driving of the three green LEDs. Since the chosen PSoC micro-controller embeds FPGA-programmable blocks, the analog front-end was entirely designed on the micro-controller, with no external components required on the PCB. ***PGA***: Programmable Gain Amplifier; ***TIA***: Trans-Impedance Amplifier; ***VDAC***: Voltage Digital to Analog Converter.

frequency of 2KHz for 16-bit resolution, with an internal reference voltage (V_{ref}). The front-end of the PPG signal was set in photo-voltaic configuration (current-to-voltage converter) and therefore connected to a trans-impedance amplifier (TIA), featuring the positive pin to ground voltage. Similarly to the PCG front-end, a DAC (VDAC_1 in Fig. 5) was adopted to drive the negative pin of the ADC, in order to reduce the dark current noise. Here, a successive approximation converter (SAR) ADC, featuring 12-bits of resolution and a sampling rate of 10KHz, was adopted. As detailed below, both DAC signal biases were automatically tuned by means of devoted procedure at the device power-on. For each of the two ADCs, one interrupt service routine was issued at the end of the ADC conversion (EOC) and captured data were transferred into a circular buffer allocated in the PSoC RAM. In order to ensure the synchronization between the PCG and PPG signals, sampled at 2kHz and 10kHz, respectively, a timer block was implemented to trigger the data storage into the memory with a period of 1ms, as depicted in Fig. 6. At trigger time, the sampled data of each signal, collected so far in the buffer, were averaged and then stored using a two-byte word. This averaging procedure, that could be achieved with the use of two different sampling frequencies of the ADCs, allowed to smooth the measured analog signals. The tuning of the DAC voltage bias (b_{DAC}) was performed by first setting the voltage internal range ΔV of the ADC to 0-5V, with a reference voltage V_{ref} of 1024mV, to allow a wide span of the input. As many as 5000 signal samples (gathering time 5ms) were retained to compute an average value $\bar{v}$.

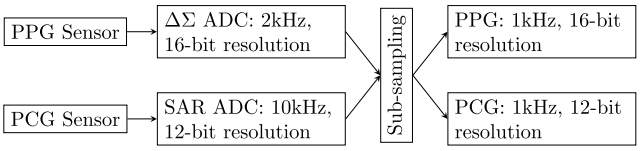

FIGURE 6. Block diagram of the ADC subsampling process.

This value was then mapped into the maximum voltage amplitude of the 8-bit DAC (4080mV) to obtain the final DAC level as:

$$b_{DAC} = \bar{v} \cdot \frac{\Delta V}{d} \cdot \frac{255}{4080} \tag{5}$$

where d was the ADC resolution. From this point on, the continuous value b_{DAC} was generated by the DAC (Fig. 5) and the ADC internal reference range was set to $\pm V_{ref}$ to optimize the sampling resolution on the signal amplitude.

D. SIGNAL PROCESSING FOR HR AND VTT COMPUTATION

After the on-board acquisition and storage of the PCG and PPG signals, data were transferred and then processed offline with Matlab (Mathworks, USA). The following digital filter configurations were used to clean out noise from the signals:

- *PCG:* 4^{th} order band-pass Butterworth filter, with cut-off frequencies of 1.5 and 40 Hz;
- *PPG:* 4^{th} order band-pass Butterworth filter, with cut-off frequencies of 0.5 and 20 Hz.

These filter configurations allowed to remove both the low frequency components due to breathing, and the high frequency effects of muscle vibrations and residual heart sounds. In order to obtain a zero-phase shift, the two filters were applied in a forward-backward configuration. After filtering, the first heart sound $S1$ and the PPG signal foot had to be extracted from the PCG and PPG signals, respectively.

1) S1 SOUND DETECTION

In order to correctly estimate PAT from PCG and PPG signals, the first heart sound, $S1$, had to be extracted from the PCG signal. A simple double threshold approach was implemented, in order to ease the future real-time on-board implementation of $S1$ detection. As a first step, the filtered PCG signal was differentiated to enhance the typical biphasic shape of the sound. Then, all the positive and negative peaks present in the signal were identified, and their average values were computed ($\text{T}_{1,p}$ and $\text{T}_{2,n}$). After this first peak identification, only the peaks above $\text{T}_{1,p}$ and below $\text{T}_{1,n}$ were considered, and their average value was again computed ($\text{T}_{2,p}$ and $\text{T}_{2,n}$). After the identification of the thresholds, all the negative peaks below $\text{T}_{2,n}$ were labeled as P_n. If, in a time interval of 70ms around the i-th P_n, a positive peak with an amplitude greater than $\text{T}_{2,p}$ was found, then the zero crossing point between the negative and the positive peak was labeled as heart sound $S1$. In order to make this identification more robust, a cross correlation technique was used to double check the correctness of the heart sound detection. The first

5 detected heart sounds $S1$ were used as reference signals, and the cross correlation between each detected heart sound and the reference heart sounds was computed. The three heart sounds that showed the highest values of cross correlation were aligned, averaged and used as reference. After this procedure, cross correlation was computed again and only those heart sounds that showed a cross-correlation higher than the maximum value were considered as true heart sounds.

2) PPG FOOT DETECTION

The second step towards the PAT estimation was the PPG foot detection. As shown in Fig. 1, PAT is computed as the time difference between the heart sound $S1$ and the PPG foot. The detection of the PPG foot was thus performed by exploiting the S1 event detected on the PCG signal. As soon as S1 event was correctly detected, the corresponding event was projected on the PPG signal. From this time point on, a time window 272ms long was analyzed. This value was chosen considering a maximum heart rate of 220 beats per minute (bpm), which is equivalent to one beat every 272 ms. Inside this time window, the first minimum value of the PPG signal, other than the boundary of the time window, was considered as the PPG signal foot.

E. BP MODEL AND CALIBRATION

The BP model defined in (4) was specified considering a linear relation between BP and HR, in agreement with [29], [35], as:

$$BP = \alpha \ln PAT + \beta HR + \gamma \tag{6}$$

where PAT and HR are expressed in ms and beat/s, respectively, whereas BP in expressed in mmHg. A calibration procedure for computing the three parameters (α, β and γ) was developed by recording reference values of BP using the GIMA ABPM holter pressure monitor (GIMA, Italy). The acquisition protocol required the holter cuff placed at the right arm of the subject and the device attached at the chest by an elastic band (Fig. 7) for concurrent data acquisition of PGC and PPG. One single registration of SBP and DBP values by the holter system required, on average, a total of 20 seconds. When the two BP measures became available, the operator triggered the device by sending a command via BLE in order to annotate the PCG and PPG signals with the correspondent time instant. After completing the recording, data from SD card were read and processed offline to compute the corresponding HR and PAT values. Using at least four BP references values, model parameters were assessed by least-square optimization.

F. DEVICE POSITIONING AND REAL-TIME FEEDBACK

As previously described, the shape of the device complied with the natural curvature of the breast and the sternum area. At setup time, the clinical operator was required to position the device on the human subject skin and started it in setup mode. In this functional mode, the original signals acquired at 1KHz were delivered through BLE in packets of 20 samples

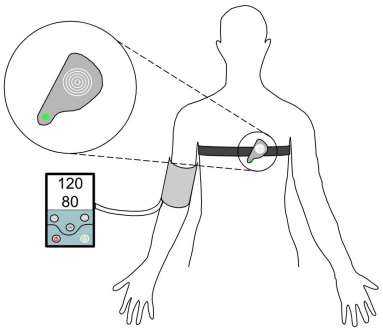

FIGURE 7. Experimental setup of the measures, with the device coupled to the chest of the subject through an elastic band and the cuff of the GIMA ABPM at the right arm. The optical system and the sensor bell of the device were attached to the skin.

at a streaming rate of 50Hz to the host computer. An internal 20ms timer drove this process. The data collected in this phase were used by the operator only to visualize and inspect the signals to qualitatively assess the signal patterns and the eventual presence of noise or interference. By slightly changing the orientation of the device, the operator could check for signal quality improvement, thus easing the post processing. In addition to the position and orientation of the device, the duty cycle of the PWM controlling the green LEDs could be tailored and personalized for each subject, according to his/her skin properties. Once the signals were considered to be satisfactory, the operator positioned, in a definite way, the device on the subject skin through an elastic band, and switched the device functioning mode to normal acquisition.

III. EXPERIMENTAL TESTS AND RESULTS

A. TESTING PROTOCOL

A total of 20 adult volunteers (8 females and 12 males), aged 24-37 years without known cardiovascular anomalies, were recruited to participate in this study. The experimental procedures followed the principles outlined in the Helsinki Declaration of 1975, as revised in 2000. All subject were provided with all the required information about the experiments and they were asked to sign an informed consent prior to the experiments. The protocol for the experiments was divided in three main phases, namely system setup, data acquisition for model calibration, and data acquisition for model validation.

1) System setup: the main purpose of this phase was to acquaint the participant with the testing condition and to setup the system. In this phase, the participant was required to seat comfortably on a chair for about two minutes, wearing both the cuff of the GIMA ABPM Holter pressure apparatus and the developed device. The device was positioned on the lower part of the sternum, slightly tilted with respect to the vertical direction (Fig. 7). This position was justified by two main considerations: the bell embedding the pressure sensor opening had to be positioned as close as possible to the heart while the optical system had to be placed at the sternum, which is known to be well vascularized. A visual inspection of the PCG and PPG signals acquired by the device allowed to adjust and optimize the device position.

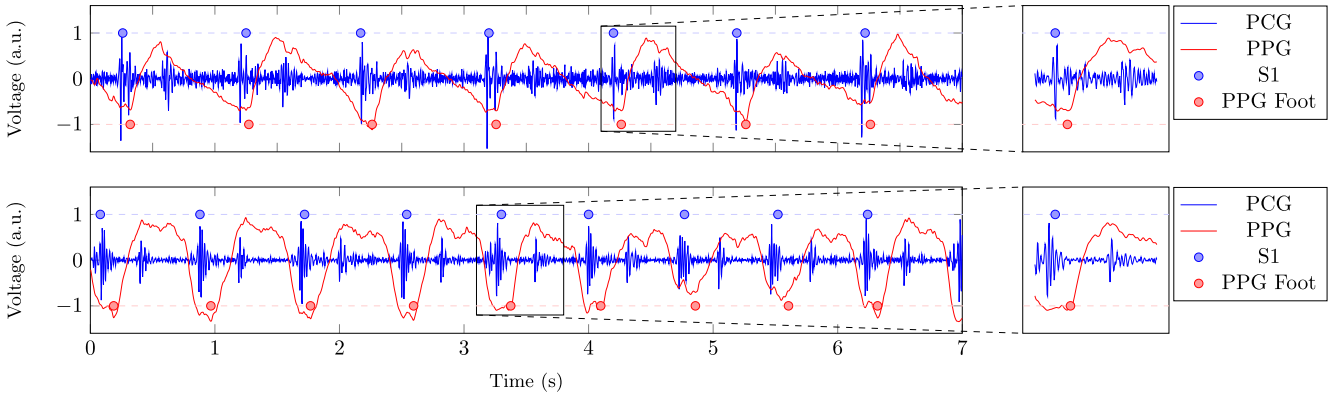

FIGURE 8. Example of data recorded from two participants involved in the experiments. Upper panel: male subejct; lower panel: female subject. The data presented are the PPG (red) and PCG (blue) signals filtered and normalized over a 7 seconds window. In addition to the PPG and PCG signals, the S1 (blue dots) and PPG foot (red dots) timepoints detected with the described algorithm are shown. On the right of the figure, a shorter time window of 0.6 seconds highlights the detected S1 heart sound and the PPG foot.

2) Calibration data acquisition: in the second phase, four measures were taken from both systems concurrently while the participant took up different postures (sitting, sitting with raised arms, standing, standing with raised arms), with each posture lasting two minutes. The collected measures were then used for model calibration (6). After calibration, four values of DBP and SBP for each participant were computed. For a subset of six participants, four additional measures for calibration were attained. This was motivated by the possibility of improving BP measurement accuracy when increasing the calibration points.

3) Validation data acquisition: in the third phase, five blood pressure measurements were collected, again from both the Holter pressure monitor and the developed device, in order to test the extrapolation quality of the algorithm for BP estimation. The data collected in this third phase were not used for calibration of the subject-specific model.

A subgroup of 17 out of 20 participants was recruited, at the end of the experiment, to perform an assessment of the ergonomics and user friendliness of the device. This was done in order to understand if the device could potentially be used without the supervision of a clinician in daily life. At first, the participants were taught how to correctly position the device on the chest, as if they were reading the user manual of the device. After this, they were asked to position it on the chest, and perform a visual inspection of both PPG and PCG signals on the user interface. Once they reached a satisfying PPG signal, they started to slightly turn the device in order to achieve a good result also in terms of PCG signal quality. The total number of attempts, the final positioning angle of the device and the time spent before completing the trial were annotated. The ergonomics of the device was evaluated by the participants on a 5 point scale (1-5, with 1 being totally uncomfortable and 5 very comfortable). The quality of the PCG and PPG signals was evaluated by the experimenters on a qualitative scale (1-5, with 1 meaning low quality signals, and 5 optimal signals). The overall experiment lasted for a maximum of 30 minutes, according to the number of measurements performed with each participant. The agreement between the reference and the estimated BP was analyzed according to the Bland-Altman approach, considering the consistency limits defined by mean±1.96SD.

TABLE 3. Results of the peak detection for the PCG and PPG signals. *CR:* Correct Recognition; *WR:* Wrong Recognition; *MR:* Missed Recognition.

	1^{st} Window	2^{nd} Window	3^{rd} Window	Total
		PCG		
CR	87.1%	94.2%	92.4%	91.2%
WR	0.4%	0.6%	0.6%	0.5%
MR	12.5%	5.2%	7%	8.3%
		PPG		
CR	96.5%	99.1%	99.2%	98.4%
WR	2%	0.8%	0.5%	1%
MR	1.5%	0.1%	0.3%	0.6%

B. PEAK RECOGNITION

The raw recorded data of 6 subjects were manually inspected in order to quantify the robustness of the automatic algorithm for the detection of heart sound *S*1 and of the PPG signal foot. An example of the PCG and PPG signals recorded with the proposed device is shown in Fig. 8. For each subject, three synchronized time windows of 100 seconds of the PCG and PPG signals were randomly chosen from the data recorded during the measurement sessions. The first window was randomly chosen in the first third of the recording session, the second window in the second third, and the last window in the last third. These data were analyzed both by the developed algorithm and manually by the authors. The results of this analysis on peak detection are reported in Table 3. On an overall number of 3700 analyzed heart beats, corresponding to more or less 1 hour of continuous registration, a sensitivity of 91.7% was reached for the heart sound detection, and 99.4% for the PPG signal foot identification.

C. HEART RATE DETECTION

Bland-Atlman analysis was performed on HR measurements. The range of measured HR values was 53-110 bpm.

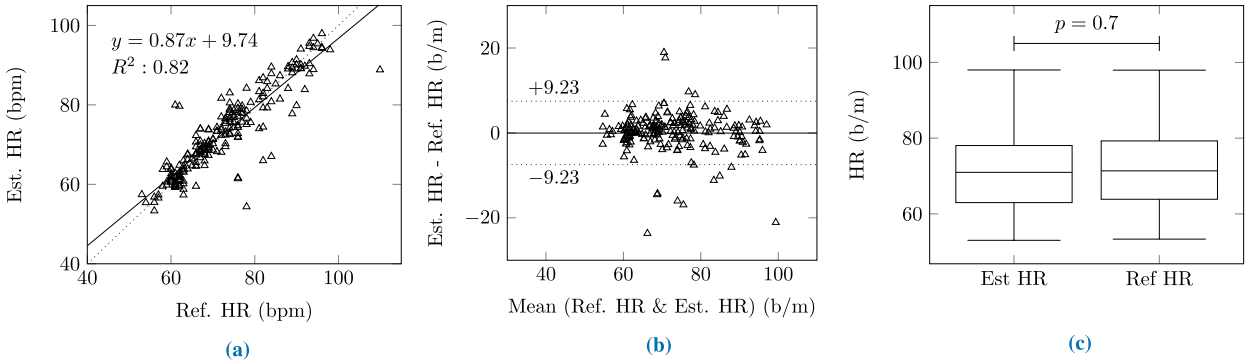

FIGURE 9. a) and b): Bland Altman plots for heart rate analysis. Reference values (Ref. HR) were obtained with the GIMA ABPM Holter pressure monitor, while estimated values (Est. HR) were computed starting from heart sound *S*1 detection. The equation in the plot at the top of the figure represents the linear regression curve for the estimated heart rate values. c): Boxplot of similarity analysis with Wilcoxon paired test for the HR measurements. *b/m:* bpm.

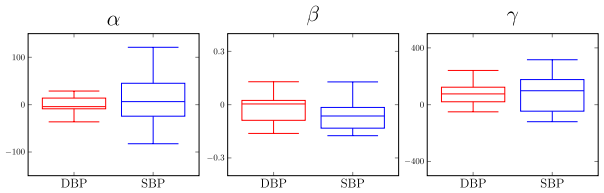

FIGURE 10. Boxplots showing the distributions of the α, β, and γ parameters of the estimated model, as described in Eq. (6), using a 4-point calibration procedure.

Fig. 9a and Fig. 9b show the result of this analysis. Reference values for HR were obtained with the same holter system used to get reference pressure values, while estimated HR was computed starting from the detection of the first heart sounds *S*1. Bland-Altman analysis showed that the mean standard deviation for the estimated HR against reference HR was 0.2±9.23 bpm. The R^2 value for the linear regression curve estimated from HR measurements was equal to 0.82. After checking the normality of the obtained data with a Lilliefors test (check HR distribution in Fig. 9a), a similarity analysis, carried out with Wilcoxon paired test, showed that there were no significant differences between the two distributions ($p = 0.7$), as shown in Fig. 9c.

D. BLOOD PRESSURE COMPUTATION

After analyzing the results related to heart rate computation, blood pressure measurements were taken into account. The coefficients of the model described in (6) were estimated using, as reference values, the measures obtained with the GIMA ABPM Holter pressure monitor. Boxplots showing the distributions of the estimated parameters are shown in Fig. 10. We performed a Bland-Altman analysis to check the correspondence between the reference and the estimated values. Since for a smaller subset of participants 8 points were used for the calibration procedures, both the measurements obtained with a 4-point calibration and those obtained with a 8-point calibration were considered for the Bland Altman Analysis. The range of diastolic and systolic measurements used for the 4-point (8-point) calibration procedure were 52-85 (67-76) and 90-141 (121-130) mmHg, respectively. The results of this analysis are shown in Fig. 11. The R^2 value for the linear regression curve computed from the measurements obtained with a 4-point (8-point) calibration was 0.91 (0.99). The Bland Altman analysis showed that the mean standard deviation for the estimated diastolic, systolic, and mean BP values, computed using a 4-point (8-point) calibration procedure, against reference BP values, were 0.97±11.18 (0.01±7.55), 0.83±18.34 (1.47±3.76), 0.90±11.27 (0.74±4.38) mmHg, respectively. The computed mean absolute difference (MAD) between the estimated and reference values for the diastolic, systolic, and mean blood pressure obtained after the 4-point (8-point) calibration were 4.36 (3.06), 6.96 (1.83), 4.58 (1.80) mmHg, respectively. A similarity analysis was performed through a Wilcoxon paired test for both systolic and diastolic pressure measurements. Boxplots showing the distributions of the reference and estimated blood pressure values, obtained with 4-point and 8-point calibration procedures, are represented in Fig. 11. Only for the systolic blood pressure measurements obtained with a 8-point calibration, there was a significant difference between the estimated and reference values ($p < 0.05$) while the absolute difference was less than 2 mmHg. We evaluated the BP measurements obtained with a 4-point calibration according to the guidelines for BP monitors defined by the British Hypertension Society (BHS) [36]. The result of this evaluation are reported in Table 4. We conducted this analysis for systolic, diastolic, and mean blood pressure separately. The BHS defines the grade for BP monitors according to the cumulative percentage of errors under three main thresholds, (5, 10, and 15 mmHg). The results obtained with this preliminary setup allowed to consider the device as a grade A BP monitor for DBP and MAP, and grade C monitor for SBP measurements. As a benchmark for further evaluation of the apparatus performances, the results obtained in a work using ECG and PPG to compute the PAT were reported [12], confirming a substantial agreement with our results.

E. ERGONOMIC ASSESSMENT

The ergonomics and the user friendliness of the prototype were tested and evaluated on a cohort of 17 participants in

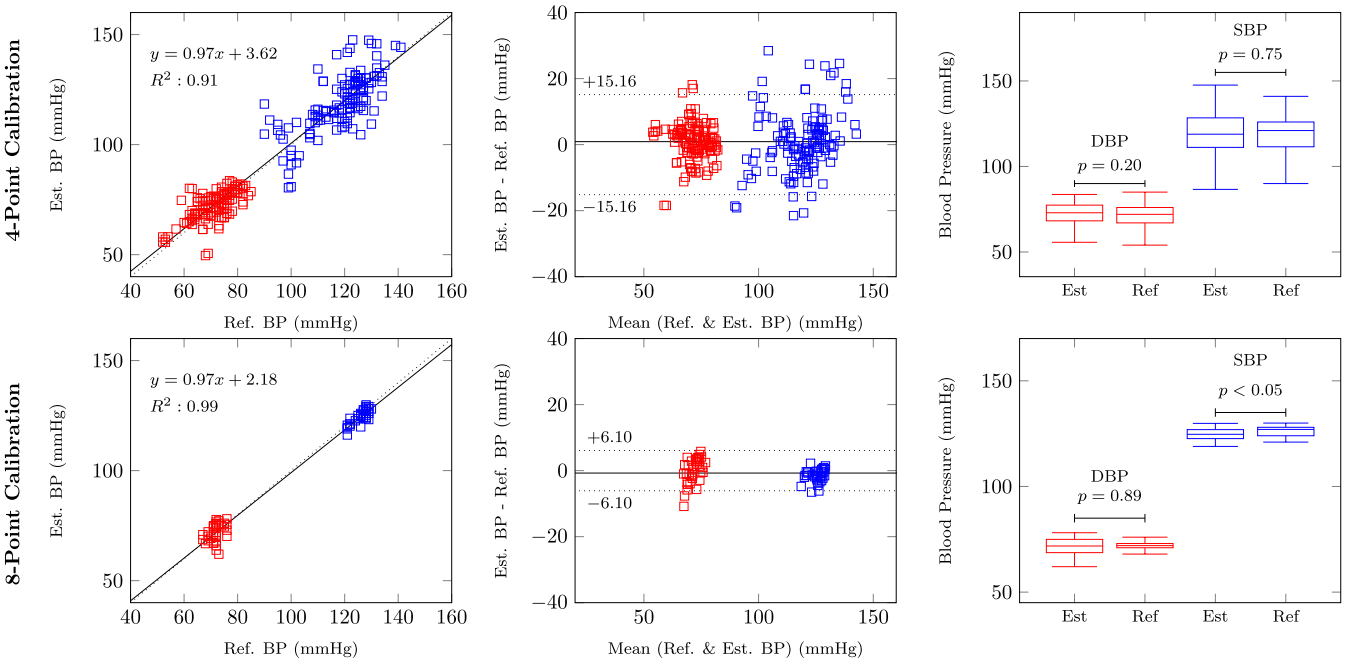

FIGURE 11. Bland-Altman and similarity analysis for blood pressure measurements. Data are shown for both diastolic (red) and systolic (blue) pressure measurements. Plots at the top (bottom) of the figure are referred to measurements estimated after a 4-point (8-point) calibration. The number of depicted samples for the 4-point calibration procedure is equal to 130, while for the 8-point calibration is 36.

TABLE 4. Comparison between the cumulative error percentages of the estimated BP measurements obtained with the proposed device, the work proposed by Kachuee *et al.* [12], and the standards defined by the BHS [36].

		Cumulative Error Percentage (%)		
		$\leq$ 5 mmHg	$\leq$ 10 mmHg	$\leq$ 15 mmHg
Device	DBP	68.4	93.9	96.2
	MAP	63.9	90.1	97.7
	SBP	49.3	76.2	86.9
[12]	DBP	62.7	87.1	95.7
	MAP	54.2	81.8	93.1
	SBP	34.1	56.6	72.7
BHS	Grade A	60	85	95
	Grade B	50	75	90
	Grade C	40	65	85

terms of optimal positioning angle, signal quality, and time required for the setup. The results of this evaluation are shown in Table 5a, 5b, and 5c. Due to the small number of participants involved in this evaluation, the analysis is qualitative and no statistical analysis was performed on the collected data. From Table 5a, it is possible to infer that results between men and women are comparable, with a difference in the positioning angle probably determined by the presence of the breast. The optimal angle for the recording was found to be around 34°, close to what was expected. Table 5b and Table 5c present the same data but from different perspectives. In particular, in Table 5b, data were reorganized according to the parameter related to the overall quality of the PPG and PCG signals. From these data, it is possible to infer that the lowest values of signal quality were found for positioning angles laying outside of the expected range (30° to 45°). Instead, Table 5c show data reorganized according to the positioning angle. The majority of the participants choose an angle between 30° and 45°.

IV. DISCUSSION

Cardiovascular diseases and the related hypertension condition are a worldwide health issue for patients, so that continuous and reliable BP monitoring is crucial for long-term diagnostic purposes [8]. From a clinical point of view, the pressure holter setup using a cuff, which consists of the automated measurement of BP every 15 to 30 minutes along a period of 24h, represents the standard (non-invasive and cost-effective) methodology in hypertension assessment and cardiovascular risk evaluation [37], [38]. However, conventional BP holter equipment, using either auscultatory or oscillometric techniques, provides BP readings at discrete time intervals and cannot support continuous measurements during daily activities. Furthermore, they may result in a discomfort to the patient as they require a mechanical perturbation of the measurement site, posing further questions about the patient adherence to the long-term monitoring [38]. The main development trend for less-obstructive BP measurement focused on solutions based on wearable devices. HeartGuide (https://www.omron-healthcare.it/) is a wearable watch, clinically validated for systolic and diastolic measures, that has been recently brought to the market by Omron (Omron Healthcare EUROPE B.V., The Netherlands). This device harnesses the oscillometric method to compute the BP and therefore it is still based on the cuff incorporating one inflatable bracelet in the strap. Such a device cannot

TABLE 5. Results on the ergonomics and user friendliness of the device. *a)*: Data grouped by gender; *b)*: data grouped by values of the quality parameter; *c)*: data grouped by values of the positioning angle parameter.

(a)

Group	Trials	Time	Quality	Angle	Ergonomics
All (*n=17*)	5.4	137 s	3.9/5	33.8°	4.3/5
Male (*n=6*)	6.2	145 s	4/5	42°	5/5
Female (*n=11*)	5.1	134 s	3.8/5	30°	3.9/5

(b)

Quality	Trials	Time	Angle	Ergonomics
Q=5 (*n=7*)	5.7	140 s	40°	4.6/5
Q=4 (*n=7*)	5	123 s	35°	3.9/5
Q<4 (*n=3*)	6.25 s	168 s	26°	4.7/5

(c)

Angle	Trials	Time	Quality	Ergonomics
0° (*n=2*)	4	90 s	3.5	5/5
30° (*n=8*)	4.5	116 s	4	4.1/5
45° (*n=4*)	7.5	207 s	3.5	3.7/5
60° (*n=2*)	6.5	127 s	4.5	5/5
90° (*n=1*)	7	146 s	4	5/5

provide continuous measurements and basically suffer from the same limitations of the traditional arm cuff holter devices. Alternatively, applanation tonometers [39], making use of volume clamp methods, and echo-tracking devices, exploiting ultrasound techniques, are intrinsically less invasive for continuous BP estimation, but, at the same time, they require a clinical setup and are elective only for patients undergoing surgery or unable to move [40]. More recently, arterial tonometry principle has been utilized into the BPro smartwatch (https://www.healthstats.com) developed by HealthSTATS Technologies (London, United Kingdom). The wrist strap of the watch embeds the force transducer and compresses the tissue and radial artery enough to cause applanation. However, for accurate measurement the fixation with adhesive tape is required. While the comparison with auscultatory reference measurements provided good agreement in a static ambulatory setup (±5 mmHg), the performance was adversely affected by motion artifact thus still preventing its usability in the daily life. Concurrently, many efforts were carried out in the development of wearable devices based on PTT/PAT. Two main types of devices can be identified: smart watches and chest devices. The smartwatch type can be further split into two sub-types, the first one using PAT, computed by ECG R-wave peak and PPG foot difference, the second one using the PTT computed from two PPG signals (wrist and fingertip). As well, chest devices can be further split into two sub-types, the first one using PAT, computed by ECG R-wave peak and PPG foot difference, the second one using PAT, computed by PCG (acoustic sensor) and PPG foot difference. The Heartisans Blood Pressure Watch (https://www.heartisans.com) is a smartwatch provided on the market by Heartisans (Hong Kong), which is based on a single differential electrocardiographic measure to detect the PTT on the PPG. Calibration with a clinical cuff-based BP device is mandatory before autonomous use. As the clinical validation has not been performed yet, the Heartisans Watch should be regarded as a consumer device. CareUp by Farasha Labs (Paris, France) is a smartwatch for BP estimation based on the PTT, measured by the time delay of the blood pulse registered by means of two photopletismography sensors, one located on the back and one on the front of the device on which the subject places the fingertip [41]. The HR, attained by the PPG detected at the finger, is used to refine the BP model, which was a linear regression of PPT and HR. The model calibration was based on repeated BP measures by sphygmomanometer. Validation performed on 44 healthy subjects provided accuracy results of diastolic and systolic BP of about 5 and 9 mmHg. However, despite clinical validation, oscillometric, tonomoter and optical wearable monitors available on the market still entail subject awareness and have not addressed yet the issues related to continuous and long-term BP measurements, which are fundamental for diagnostic monitoring [4], [6], [23]. In addition, especially for optical devices, the main weakness is that only records at rest can be performed, due to the poor stability of the PPG signal to the movements [7], [12]. Moving along the direction of detecting the BP routinely and non-invasively, in this work a chest device, based on the measure of the PCG and PPG waveforms, was proposed exploiting the relation between PTT and BP. The non-invasive BP measurement exploited in this device relies on the computation of the PAT, which was proposed as a surrogate of the PTT and showed reasonable correlation with BP [15], [16], [42]. The Moens-Korteweg model, which assumes a relation between the average intramural pressure and the PWV of elastic tubes, was simplified to express an explicit relation of both systolic and diastolic blood pressures with the PAT and HR in bundle. The development proposed in the present paper addressed some technological and functional limitations (wearability discomfort, discrete and short-term measurements to cite a few) of the traditional cuff-based systems. The work led to the implementation of a fully integrated prototype able to measure BP

in a non-invasive and continuous manner potentially without interfering with daily activities, as it can be worn easily on the chest (lightweight and small) and it does not require neither mechanical perturbations at the measurement site nor the subject active participation. In the light of the above results, the main technical contributions can be summarized as follows. First, the prototype was able to measure synchronously the PCG and the PPG signals, avoiding the explicit measure of ECG. Second, the detection of PCG was based on the seamless integration of a miniaturized pressure sensor and a custom-designed auscultatory bell, making the PCG acquisition minimally sensitive to disturbance from environmental sound noise. Third, the use of the PSoC μ-controller has allowed us to minimize the analog front-end thus increasing the quality of the signals obtained from the photodiode and pressure analog sensors. Fourth, the geometry of the device was designed to cope with chest morphology, especially to match the breast arch. As a result, none of the enrolled participants expressed distress wearing the prototype. Last, all these contributions allowed to obtain mean absolute differences of diastolic, systolic and mean BP, with respect to the reference of 4.36, 6.96 and 4.58 mmHg, respectively. From a scientific point of view, we have confirmed that the model embedding PAT and the heart rate provided BP results, attained upon subject-dependent calibration of the model parameters for a cohort of 20 healthy subjects, in a agreement with those reported in the literature adopting similar models [4], [12], [21], [22], [42], [43]. In particular, according to the BHS standard, our prototype was consistent with the grade A in the estimation of DBP and MAP values overcoming the results obtained by a similar setup [12], which featured grade B in the estimation of the MAP value. In [43], a regression model was used to relate PTT to BP reporting a SD of the mean pressure in the range of ± 3 mmHg on a cohort of 14 normotensive subjects. In [21], the authors reported a chest sensor tested in a cohort of 15 healthy subjects, exploiting the PWV principle, providing a MAD for pressure measurements in the range ± 5 mmHg. Interestingly, the sensor performance was maintained even two weeks after having performed the initial subject-dependent calibration. In [4], the author proposed an armband wearable device based on PTT reporting a SD of the mean pressure in the range of ± 8 mmHg, validated on a small cohort of 10 healthy subjects. Investigation by [11] about the photoplethysmgram intensity ratio, accounting for changes in arterial compliance, as a correction factor for PTT, revealed an improvement of the BP measurement reporting a range of about ± 3 mmHg, validated on 27 healthy subjects. An inverse model between BP and PTT was proposed in [42] attaining an accuracy of diastolic and systolic BP of about 5 and 6 mmHg, respectively. From an operational point of view, the focus on a chest device rather than a sensor watch on the wrist was dictated by physiological considerations about the relation between the PAT and the BP in the Moens-Korteweg model, which relates the speed of the fluid pulse traveling into a vessel to the compliance and geometry of the vessel. The validity of this model in the context of the human vascular tree is dependent on the assumption that the geometric regulation of the vascular bed has little influence of the transit time [21], [22]. The advantage of computing the PAT at the sternum allows to neglect the effect of arterioral autoregulation to the total transit time as the propagation of the pressure-pulse wave at the sternum vascular bed occurs at high speed [14], [18]. Therefore, the PAT measurement performed according to the described setup is expected to describe the stiffness of the elastic and large muscular arteries, combined in a single PAT value [17]. Nonetheless, the major issue with the PAT, triggered by the R-wave, is that it is not a perfect surrogate of the PTT as there is an additional time delay, traditionally called pre-ejection period (PEP), between the action of atrioventricular valve closing and the pulse wave propagation to the arterial tree. However, the use of ballistocardiography (heart sound) sensor allowed us to compute the PAT direct from the S1 sound, method that has been confirmed to minimize the influence of cardiac PEP differences [44]. Furthermore, PAT and PTT were mainly reported to be correlated with systolic than diastolic BP [23] thus posing questions about the generalization of the Moens-Korteweg model to diastolic pressure. According to recent papers in the literature [29], [30], [41] that suggested a direct dependence of the BP to the HR, the Moens-Korteweg model was extended by assuming a linear relation, as reported in (6). However, this relation is to be considered reasonable only within a small range of BP variations [45]. For instance, as the BP decreases the HR increases in an effort to augment the cardiac output, with a concurrent contraction of the arterial walls to increase the BP. Conversely, as soon as the BP increases the HR tend to decrease, along with a release of the arterial wall, to work against a potential dangerous condition [27], [28]. Moreover, the model should take into account that, as the HR increases, corresponding for example to some physical exercise, the short-term effect on the BP should be less than linear and even the BP should reach a saturation value. While, according to such basic physiological considerations, a non-linear relation, like the logistic function, would be more realistic, the complexity of dealing with multiple more parameters prevents to obtain high accuracy in the calibration with few measures. In addition, as it was shown in Fig. 10, solving the calibration using a least-square optimization can lead to high variability in the parameters, issue that can decrease the overall model accuracy when increasing the number of parameters. Some technical limitations of the work have to be discussed. In this prototype release of the device, real-time operations pertained only to the signal acquisition while data post-processing and analysis were performed off-line. Transferring signal analysis completely on-board can be feasible but it is acknowledged to be challenging as data buffer allocation in random access memory and real-time operations are to be carefully optimized to ensure accuracy in the PAT detection. The verification of the PPG waveform was performed at the device positioning time by checking qualitatively the signal in a trial-and-error procedure. Potentially, this procedure could be implemented on-board to allow

the automatic assessment of the PPG quality in terms of motion artifacts or other environmental effects, thus reducing unnecessary data transmission and saving battery power [46]. A brachial oscillometric system was used as a reference BP measurement for both model calibration and testing, introducing further uncertainty due the average BP readings along the required time period of about 20s for each measure. As the results showed, the calibration of the BP model was strongly dependent of the number of considered PAT-BP pairs. The difference between 8- and 4-point calibration, both in diastolic and systolic accuracy, suggests that increasing the number of calibration points is mandatory to ensure high accuracy, however at the expense of a higher operating cost. As far as the shape of the device is concerned, for female participants the angle for positioning the device was limited due to the the presence of the breast but the real-time feedback at positioning time allowed to maximize the signal quality. Finally we point out that the employed acquisition protocol limited the span of the BP values. We acknowledge that the Institute of Electrical, and Electronics Engineers (IEEE) has proposed a validation protocol [47] devoted to cuff-less BP monitors to cope with the AAMI standard for cuff-based devices. Such a protocol envisages the testing of the cuff-less device across a wide range of BP, including pathological conditions, and the validation of the initial calibration after a significant time period (even weeks) to investigate the stability over time of the calibration. In this preliminary work, the device was calibrated within a physiological range of blood pressures and more systematic validations are considered for future works. Furthermore, additional efforts should be made in order to improve the algorithms employed for the detection of the S1 heart sound and the PPG foot.

V. CONCLUSION

Much effort is now leading to the manufacturing of wearable devices for long-term blood pressure monitoring. Although interesting commercial products have recently been proposed, some technical and ergonomic challenges still remain unmet. As described, the innovative chest apparatus proposed in this work, designed and implemented to address some of such issues, was able to record the PCG and PPG signals, which can be processed to extract the PAT and the HR which in turn, coupled with the Moens-Korteweg model, allow to estimate the BP. While preliminary, the reported results on 20 normotensive subjects, with an accuracy comparable with traditional invasive methods, are promising and represent a starting point for future improvements, for example transferring on-board the signal processing and analysis, and further validation including hypertensive patients in a clinical controlled study. Therefore, we consider that the proposed device will be able to monitor the BP in an unobtrusive way, allowing prolonged monitoring and avoiding discomfort to achieve a better prevention and management of hypertension, thus reducing the global burden caused by cardiovascular diseases.

ACKNOWLEDGMENT

The authors would like to thank the volunteer students of the Department of Electronics, Information and Bioengineering, Politecnico di Milano for their participation in the experimental tests. They also wish to thank A. Porro and E. Vannoni for supervising the experiments.

REFERENCES

[1] X.-F. Teng and Y.-T. Zhang, "Theoretical study on the effect of sensor contact force on pulse transit time," *IEEE Trans. Biomed. Eng.*, vol. 54, no. 8, pp. 1490–1498, Aug. 2007.

[2] H. Gesche, D. Grosskurth, G. Küchler, and A. Patzak, "Continuous blood pressure measurement by using the pulse transit time: Comparison to a cuff-based method," *Eur. J. Appl. Physiol.*, vol. 112, no. 1, pp. 309–315, Jan. 2012.

[3] I. C. Jeong and J. Finkelstein, "Optimizing non-invasive blood pressure estimation using pulse transit time," *Stud. Health Technol. Inform.*, vol. 192, p. 1198, Jan. 2013.

[4] Y.-L. Zheng, B. P. Yan, Y.-T. Zhang, and C. C. Y. Poon, "An armband wearable device for overnight and cuff-less blood pressure measurement," *IEEE Trans. Biomed. Eng.*, vol. 61, no. 7, pp. 2179–2186, Jul. 2014.

[5] H. Gholamhosseini, A. Meintjes, M. Baig, and M. Linden, "Smartphone-based continuous blood pressure measurement using pulse transit time," *Stud. Health Technol. Inform.*, vol. 224, pp. 84–89, Jan. 2016.

[6] S.-H. Liu, D.-C. Cheng, and C.-H. Su, "A cuffless blood pressure measurement based on the impedance plethysmography technique," *Sensors*, vol. 17, no. 5, p. 1176, 2017.

[7] H. Gholamhosseini, M. Baig, S. Rastegar, and M. Lindén, "Cuffless blood pressure estimation using pulse transit time and photoplethysmogram intensity ratio," *Stud. Health Technol. Inform.*, vol. 249, pp. 77–83, Jan. 2018.

[8] G. S. Stergiou, P. Palatini, R. Asmar, J. P. Ioannidis, A. Kollias, P. Lacy, R. J. McManus, M. G. Myers, G. Parati, A. Shennan, J. Wang, and E. O'Brien, and European Society of Hypertension Working Group on Blood Pressure Monitoring, "Recommendations and practical guidance for performing and reporting validation studies according to the universal standard for the validation of blood pressure measuring devices by the association for the advancement of medical instrumentation/european society of hypertension/international organization for standardization (aami/esh/iso)," *J. Hypertension*, vol. 37, pp. 459–466, Mar. 2019.

[9] M. Y. M. Wong, E. Pickwell-MacPherson, Y. T. Zhang, and J. C. Y. Cheng, "The effects of pre-ejection period on post-exercise systolic blood pressure estimation using the pulse arrival time technique," *Eur. J. Appl. Physiol.*, vol. 111, no. 1, pp. 135–144, Jan. 2011.

[10] A. Patzak, Y. Mendoza, H. Gesche, and M. Konermann, "Continuous blood pressure measurement using the pulse transit time: Comparison to intra-arterial measurement," *Blood Pressure*, vol. 24, no. 4, pp. 217–221, Jul. 2015.

[11] X.-R. Ding, Y.-T. Zhang, J. Liu, W.-X. Dai, and H. K. Tsang, "Continuous cuffless blood pressure estimation using pulse transit time and photoplethysmogram intensity ratio," *IEEE Trans. Biomed. Eng.*, vol. 63, no. 5, pp. 964–972, May 2016.

[12] M. Kachuee, M. M. Kiani, H. Mohammadzade, and M. Shabany, "Cuffless blood pressure estimation algorithms for continuous health-care monitoring," *IEEE Trans. Biomed. Eng.*, vol. 64, no. 4, pp. 859–869, Apr. 2017.

[13] M. Elgendi, R. Fletcher, Y. Liang, N. Howard, N. H. Lovell, D. Abbott, K. Lim, and R. Ward, "The use of photoplethysmography for assessing hypertension," *NPJ Digit. Med.*, vol. 2, no. 1, p. 60, Dec. 2019.

[14] J. Y. A. Foo, S. J. Wilson, G. R. Williams, A. Coates, M.-A. Harris, and D. M. Cooper, "Predictive regression equations and clinical uses of peripheral pulse timing characteristics in children," *Physiolog. Meas.*, vol. 26, no. 3, pp. 317–328, Jun. 2005.

[15] M. Gao and R. Mukkamala, "Perturbationless calibration of pulse transit time to blood pressure," in *Proc. Annu. Int. Conf. IEEE Eng. Med. Biol. Soc.*, vol. 2012, Aug. 2012, pp. 232–235.

[16] R. Mukkamala, J.-O. Hahn, O. T. Inan, L. K. Mestha, C.-S. Kim, H. Toreyin, and S. Kyal, "Toward ubiquitous blood pressure monitoring via pulse transit time: Theory and practice," *IEEE Trans. Biomed. Eng.*, vol. 62, no. 8, pp. 1879–1901, Aug. 2015.

[17] E. G. Brennan, N. J. O'Hare, and M. J. Walsh, "Transventricular pressure-velocity wave propagation in diastole: Adherence to the moens-Korteweg equation," *Physiolog. Meas.*, vol. 19, no. 1, pp. 117–123, Feb. 1998.
[18] D. Shahmirzadi, R. X. Li, and E. E. Konofagou, "Pulse-wave propagation in straight-geometry vessels for stiffness estimation: Theory, simulations, phantoms and in vitro findings," *J. Biomech. Eng.*, vol. 134, no. 11, Nov. 2012, Art. no. 114502.
[19] J. Allen, "Photoplethysmography and its application in clinical physiological measurement," *Physiolog. Meas.*, vol. 28, no. 3, pp. R1–R39, Mar. 2007.
[20] J. Sola, S. F. Rimoldi, and Y. Allemann, "Ambulatory monitoring of the cardiovascular system: The role of pulse wave velocity," in *New Developments in Biomedical Engineering*, D. Campolo, Ed. Rijeka, Croatia: IntechOpen, 2010, ch. 21, pp. 391–424, doi: 10.5772/7608.
[21] J. Sola, M. Proenca, D. Ferrario, J.-A. Porchet, A. Falhi, O. Grossenbacher, Y. Allemann, S. F. Rimoldi, and C. Sartori, "Noninvasive and nonocclusive blood pressure estimation via a chest sensor," *IEEE Trans. Biomed. Eng.*, vol. 60, no. 12, pp. 3505–3513, Dec. 2013.
[22] F. Heydari, M. P. Ebrahim, J.-M. Redoute, K. Joe, K. Walker, and M. Rasit Yuce, "A chest-based continuous cuffless blood pressure method: Estimation and evaluation using multiple body sensors," *Inf. Fusion*, vol. 54, pp. 119–127, Feb. 2020.
[23] J. Y. A. Foo, C. S. Lim, and P. Wang, "Evaluation of blood pressure changes using vascular transit time," *Physiolog. Meas.*, vol. 27, no. 8, pp. 685–694, Aug. 2006.
[24] M. Y. M. Wong, C. C. Y. Poon, and Y. T. Zhang, "Can the timing-characteristics of phonocardiographic signal be used for cuffless systolic blood pressure estimation?" in *Proc. Int. Conf. IEEE Eng. Med. Biol. Soc.*, vol. 1, Aug. 2006, pp. 2878–2879.
[25] F. S. Cattivelli and H. Garudadri, "Noninvasive cuffless estimation of blood pressure from pulse arrival time and heart rate with adaptive calibration," in *Proc. 6th Int. Workshop Wearable Implant. Body Sensor Netw.*, Jun. 2009, pp. 114–119.
[26] R. Wang, W. Jia, Z.-H. Mao, R. J. Sclabassi, and M. Sun, "Cuff-free blood pressure estimation using pulse transit time and heart rate," in *Proc. 12th Int. Conf. Signal Process. (ICSP)*, vol. 2014, Oct. 2014, pp. 115–118.
[27] A. C. Guyton, "The relationship of cardiac output and arterial pressure control," *Circulation*, vol. 64, no. 6, pp. 1079–1088, Dec. 1981.
[28] T. Ma and Y. T. Zhang, "A correlation study on the variabilities in pulse transit time, blood pressure, and heart rate recorded simultaneously from healthy subjects," in *Proc. IEEE Eng. Med. Biol. 27th Annu. Conf.*, Jan. 2005, pp. 996–999.
[29] S. Reule and P. E. Drawz, "Heart rate and blood pressure: Any possible implications for management of hypertension?" *Current Hypertension Rep.*, vol. 14, no. 6, pp. 478–484, Dec. 2012.
[30] P. Zhang, Q. Qiu, Y. Luo, Y. Zhou, and J. Liu, "A simple method for reconstruction of continuous brachial artery pressure from continuous digital artery pressure in humans," in *Proc. 39th Annu. Int. Conf. IEEE Eng. Med. Biol. Soc. (EMBC)*, Jul. 2017, pp. 1696–1699.
[31] N. Selvaraj and H. Reddivari, "Feasibility of noninvasive blood pressure measurement using a chest-worn patch sensor," in *Proc. 40th Annu. Int. Conf. IEEE Eng. Med. Biol. Soc. (EMBC)*, vol. 2018, Jul. 2018, pp. 1–4.
[32] Y. Maeda, M. Sekine, and T. Tamura, "The advantages of wearable green reflected photoplethysmography," *J. Med. Syst.*, vol. 35, no. 5, pp. 829–834, Oct. 2011.
[33] M. R. Grubb, J. Carpenter, J. A. Crowe, J. Teoh, N. Marlow, C. Ward, C. Mann, D. Sharkey, and B. R. Hayes-Gill, "Forehead reflectance photoplethysmography to monitor heart rate: Preliminary results from neonatal patients," *Physiolog. Meas.*, vol. 35, no. 5, pp. 881–893, May 2014.
[34] J. Harju, A. Tarniceriu, J. Parak, A. Vehkaoja, A. Yli-Hankala, and I. Korhonen, "Monitoring of heart rate and inter-beat intervals with wrist plethysmography in patients with atrial fibrillation," *Physiolog. Meas.*, vol. 39, no. 6, Jun. 2018, Art. no. 065007.
[35] J.-F. Morcet, M. Safar, F. Thomas, L. Guize, and A. Benetos, "Associations between heart rate and other risk factors in a large french population," *J. Hypertension*, vol. 17, no. 12, pp. 1671–1676, Dec. 1999.
[36] E. O'Brien, B. Waeber, G. Parati, J. Staessen, and M. G. Myers, "Blood pressure measuring devices: Recommendations of the European society of hypertension," *BMJ*, vol. 322, no. 7285, pp. 531–536, Mar. 2001.
[37] E. O'Brien, "Prognostic value of ambulatory blood pressure monitoring in obese patients," *J. Clin. Hypertension*, vol. 18, no. 2, pp. 119–120, Feb. 2016.
[38] E. O'Brien, "The lancet commission on hypertension: Addressing the global burden of raised blood pressure on current and future generations," *J. Clin. Hypertension*, vol. 19, no. 6, pp. 564–568, Jun. 2017.
[39] D. M. Bard, J. I. Joseph, and N. van Helmond, "Cuff-less methods for blood pressure telemonitoring," *Frontiers Cardiovascular Med.*, vol. 6, p. 40, Apr. 2019.
[40] L. M. Van Bortel, E. J. Balkestein, J. J. van der Heijden-Spek, F. H. Vanmolkot, J. A. Staessen, J. A. Kragten, J. W. Vredeveld, M. E. Safar, H. A. S. Boudier, and A. P. Hoeks, "Non-invasive assessment of local arterial pulse pressure: Comparison of applanation tonometry and echo-tracking," *J. Hypertension*, vol. 19, no. 6, pp. 1037–1044, Jun. 2001.
[41] R. Lazazzera, Y. Belhaj, and G. Carrault, "A new wearable device for blood pressure estimation using photoplethysmogram," *Sensors*, vol. 19, no. 11, p. 2557, 2019.
[42] A. Esmaili, M. Kachuee, and M. Shabany, "Nonlinear cuffless blood pressure estimation of healthy subjects using pulse transit time and arrival time," *IEEE Trans. Instrum. Meas.*, vol. 66, no. 12, pp. 3299–3308, Dec. 2017.
[43] M. Y.-M. Wong, C. C.-Y. Poon, and Y.-T. Zhang, "An evaluation of the cuffless blood pressure estimation based on pulse transit time technique: A half year study on normotensive subjects," *Cardiovascular Eng.*, vol. 9, no. 1, pp. 32–38, Mar. 2009.
[44] S. L.-O. Martin, A. M. Carek, C.-S. Kim, H. Ashouri, O. T. Inan, J.-O. Hahn, and R. Mukkamala, "Weighing scale-based pulse transit time is a superior marker of blood pressure than conventional pulse arrival time," *Sci. Rep.*, vol. 6, no. 1, p. 39273, Dec. 2016.
[45] B. M. McCarthy, C. J. Vaughan, B. O'Flynn, A. Mathewson, and C. Ó. Mathúna, "An examination of calibration intervals required for accurately tracking blood pressure using pulse transit time algorithms," *J. Hum. Hypertension*, vol. 27, no. 12, pp. 744–750, Dec. 2013.
[46] K. Li, S. Warren, and B. Natarajan, "Onboard tagging for real-time quality assessment of photoplethysmograms acquired by a wireless reflectance pulse oximeter," *IEEE Trans. Biomed. Circuits Syst.*, vol. 6, no. 1, pp. 54–63, Feb. 2012.
[47] *IEEE Standard For Wearable Cuffless Blood Pressure Measuring Devices*, Standard 1708-2014, Aug. 2014, pp. 1708–2014.

DAVIDE MARZORATI received the M.Sc. degree in biomedical engineering, in 2017. He is currently pursuing the Ph.D. degree in biomedical engineering with Politecnico di Milano. His main research activities focus on the development of sensors and devices for exhaled breath analysis with the aim of early disease diagnosis.

DARIO BOVIO received the B.Sc. degree in biomedical engineering, in 2006. He is a Scientific Consultant with Politecnico di Milano. He is also the Founder and CTO of Biocubica SRL, Milan, Italy, a company specialized in the development of embedded systems in the field of biomedical technology. His technological interests span biomedical sensors and embedded systems for biomedical applications.

CATERINA SALITO received the M.Sc. degree in biomedical engineering, in 2005, and the Ph.D. degree in bioengineering, in 2010. She is currently a Postdoctoral Fellow with the Department of Electronics, Information and Bioengineering, Politecnico di Milano. She is also the Co-Founder and CEO with Biocubica SRL. Her main research activities span innovative technologies for quantitative analysis of biomedical signals with special focus on respiration.

LUCA MAINARDI received the M.Sc. degree in electronics engineering, in 1990, and the Ph.D. degree in bioengineering, in 1996. He is currently a Professor with the Department of Electronics, Information, and Bioengineering, Politecnico di Milano, Italy, and the Co-Chair of the SPiNlabS Laboratory. His research activity is in the field of biomedical signal and image processing, and biomedical system modeling with applications to the cardiovascular systems. He is author of more than 120 peer-reviewed articles on international journals and more than 140 conference papers. He authored 12 book chapters and is editor of the book *Understanding Atrial Fibrillation: The Signal Processing Contribute* (Morgan and Claypool).

Dr. Mainardi is the Chair of the IEEE EMBS Technical Committee on Biomedical Signal Processing and a member of the Board of Computing in Cardiology (CinC) annual Conference. He is the Coordinator of the EU Marie-Curie project MY-ATRIA under the H2020 program framework (GA-766082).

PIETRO CERVERI received the M.Sc. degree in electronics engineering, in 1994, and the Ph.D. degree in bioengineering, in 2001. He has been an Associate Professor in bioengineering with Politecnico di Milano, since 2015. His research activities are mainly about technologies for biomedical applications with special focus on diagnosis and therapy. He is author/coauthor of more than 100 scientific articles published on ISI journals. In 2008, he was awarded with Best Innovation Award at K-Idea—Scientific Technological Park Kilometro Rosso, Bergamo, Italy, for Robotic technologies for the vision in mini-invasive transluminal endoscopic surgery. Since 2012, he has been collaborating with the National Center of Oncologic Hadron-therapy, Pave, Italy.